STUDY ON 50 MHZ ICP TORCH WITH MEDIUM RESOLUTION SPECTROMETER. DETERMINATION OF RARE EARTH ELEMENTS IN COMPLICATED MATRICES

Viktor KANICKÝ[a], Jiří TOMAN[b], Vítězslav OTRUBA[c] and Lumír SOMMER[c]

[a] *Department of Chemistry, Faculty of Education, Masaryk University, Poříčí 7, 603 00 Brno*

[b] *Geological Survey UNIGEO, Polní 23/25, 639 00 Brno*

[c] *Department of Analytical Chemistry, Masaryk University, 611 37 Brno*

Received May 19, 1992
Accepted June 14, 1992

ICP-OES is a suitable method for the determination of R.E.E. (rare earth elements), which exhibits advantages in the absence of interferences of evaporation, low detection limits and a great linear range of calibration graphs. A spectrometer having spectral bandwidth (SBW) 30 pm with the 50 MHz ICP source were used. Optimum working conditions resulted from detailed studies of axial intensity distributions. Differences in axial intensity distribution were evident when compared with usual 27.12 MHz ICP sources. Matrix interferences of alkaline salts and acids have been evaluated and the optimum spectral lines selected respecting mutual spectral interferences of R.E.E.

Hitherto, ICP-OES is widely used for the determination of R.E.E. in rocks[1 - 7], alloys[8] and in ores, their oxidic and hydroxidic concentrates and semi-finished products of material separation of R.E.E. oxides utilized for luminophores and semiconductor products[9 - 13]. While the separation of the R.E.E. group from the matrix elements of geological materials is required for determining their normal abundances[1,6,7], mutual spectral interferences of R.E.E. and their proper corrections are of primary importance for determining individual components in R.E.E. ore concentrates and mixtures of R.E.E. oxides at various ratios[13 - 16]. Available spectral tables and atlases for ICP optical emission spectrometry[17 - 19] include partially completed information on prominent analytical lines of R.E.E. in the form of spectral scans[13] or tables of correction factors[15]. Useful information for R.E.E. lines identification is provided by specialized tables[20]. Medium resolution spectrometers should be used with caution for the determination of R.E.E. in their mixtures[13].

The ICP generators operated at 27.12 MHz have been used predominantly in current ICP-OES equipments, so far. Due to differences in electron density and temperature, spatial distributions between 27.12 MHz and 50 MHz ICP discharges[21], different spatial intensity distributions of spectral lines can be expected using the 50 MHz ICP source, in comparison to 27.12 MHz one. The optimization of operating conditions of the 50 MHz ICP source during simultaneous multielement analysis was performed by

Boumans[22]. However, a detailed study of parameters such as power input, gas flow rates and observation heights for particular prominent analytical lines of R.E.E. has not been published so far for the 50 MHz ICP excitation source frequently used for contemporaneous instruments.

In this paper, the optimization of operating conditions of the 50 MHz ICP excitation source is described for simultaneous determination of R.E.E. in complicated matrices and the influence of alkali metal salts and acids on line emission. The axial intensity distributions of some lines in a 50 MHz ICP source are evaluated and compared with results for 27.12 MHz ICP sources. Analytical lines of R.E.E. with minimum spectral interferences have been selected. Contributions of interfering lines and background to the emission intensities of analytical lines were corrected using a suitable computation procedure. Procedure for the determination of R.E.E. has been developed and its accuracy tested on several reference materials.

EXPERIMENTAL

Chemicals and Solutions

Stock solutions of R.E.E. were prepared from purest R.E.E. oxides (Specpure, Johnson and Matthey, Typpi OY) by dissolving in dilute HCl (1 : 1, v/v) or in a mixture of HCl and HNO_3. Prior to dissolution the oxides were ignited at 950 °C to achieve defined stoichiometry. Ignited CeO_2 was dissolved in 45% HBr. The resulting concentration of acids in stock solutions was adjusted to 0.2 mol l^{-1} HCl and 0.3 mol l^{-1} HNO_3. The solutions were standardized by EDTA titrations and checked for other R.E.E. impurities by ICP-OES. They contained 1 or 10 mg ml^{-1} of R.E.E. Stock solutions of Li, Na, K, Ca, Mg, Sr, Ba, Al were nitrates. SiO_2 stock solution (2 mg ml^{-1} SiO_2) was prepared by melting 2 g SiO_2 with 8 g $LiBO_2$ (Spectromelt A 20, Merck Darmstadt) and dissolving the resulting melt in 0.7 mol l^{-1} HNO_3 under stirring. All chemicals used were of analytical grade purity.

Instrumentation and Operating Conditions

ICP Spectrometer Philips PV 8210 in Paschen–Runge mounting, with 30 fixed channels and a sequential PV 8280 roving detector controlled manually. Source imaged onto the grating by a spherical lens with focal length 200 mm. Ruled grating 40 × 78 mm, r = 1 500 mm , blazed for 450 nm, 1 200 grooves/mm, $1/R$ = 0.555 nm/mm; slits: entrance 20 μm, exit 50 μm (1st order) or 100 μm (2nd order); practical SBW is 35 pm; filter WG 1 (Zeiss, Jena) for the range above 400 nm; photomultipliers 1P 28, PV 8280 scanning rate adjusted to 0.3 nm min^{-1}, scans performed in the range of 0.3 – 0.5 nm; measuring unit Philips PV 8650; signal recording – X-Y recorder Philips PM 8131 operated by the control unit of the detector PV 8280, time constant 0.5 s, linear scale only.

Plasma generator Philips PV 8490, 50 MHz, free running, variable power input (0.7 – 2.2 kW), compact plasma torch, type 36 Philips, maximum adjustable gas flow rates, Ar (l min^{-1}): outer plasma 25, intermediate 6.5, aerosol carrier 2.5.

The concentric glass nebulizer Meinhard T 200 A3; dual cylindrical spray chamber (Scott type); the peristaltic pump Gilson Minipuls 2 (Gilson, France). Sample uptake: 0.8 ml min^{-1} with peristaltic pump.

Observation zone: 4 mm high, confined vertically with an intermediate screen, the width of the zone was limited by the grating frame to 13 mm. The observation height was adjusted manually within the range

8 – 28 mm above the top of the load coil. The whole torch compartment was shifted up or down perpendicularly to the optical axis using a rigid screw provided with one-milimeter lead.

Axial intensity distributions were measured at observation heights 8, 12, 16, 20, 24 and 28 mm. Integration times from 5 to 20 s were used during these measurements in order to minimize the quantizing error. Prior to modifying the integration time, its influence on the precision was evaluated. A peak-on signal integration (typically 10 s) was being performed without peak-off background correction, with preflush 60 s. A peak-on measurement of the background during nebulizing a blank solution was employed. Graphical plots of axial intensity distributions were drawn after intensity normalization.

Precision and repeatibility measurements: The precision was evaluated from the set of 10 consecutive measurements. The short-term repeatability was defined for one shift, i.e. the time interval of 8 h. Power input, gas flow rates and an observation height were always newly set for these measurements, the plasma discharge started repeatedly. After 4 and 8 h the position of the entrance slit was checked, the optical drift varied between 2 – 3 pm only. After these checks, new setting of the entrance slit position was performed to guarantee the measurement in the area of maximum of the instrumental line profile. A set of 10 measurements has been evaluated. The long-term repeatibility data acquisition has been performed in the course of 4 years at 5-month intervals and the set of 10 values was used for the RSD calculation.

Lines of lanthanoids were measured sequentially using the PV 8280 detector. Fixed channels of PV 8210 were used for common elements (Ca, Sr, Ba, Fe, Ti, Al) and Y II 371.030 mm.

Optimization Criteria

Optimized conditions for the measurement correspond to the maximum signal-to-background ratio and minimum matrix interferences. The background equivalent concentration *BEC* which is the reciprocal value of the signal-to-background ratio, was used throughout this work:

$$BEC = I_B(I_L/c_A)^{-1}, \qquad (1)$$

where I_B is the background intensity, I_L the analyte line intensity corresponding to the analyte concentration c_A.

The following relationship exists between *BEC* and the limit of detection c_L

$$c_L = 3s_B(I_L/c_A)^{-1} = 3s_{B,r}\, I_B(I_L/c_A)^{-1} = 3s_{B,r}\, BEC, \qquad (2)$$

where $s_{B,r}$ is the relative standard deviation of the background intensity I_B. The definition of the limit of detection is based on threefold of the standard deviation s_B of the background intensity[23].

For the maximum of the plot of the dependence of I_L on operating conditions, an optimum stability of a signal and precision of a slope of a calibration line are achieved.

The magnitude of the matrix interference (multiplicative interference) is expressed as a ratio

$$X = I_L^M/I_L, \qquad (3)$$

where I_L is the net line intensity for a pure analyte solution and I_L^M is the net line intensity for the analyte in a matrix.

Selection of R.E.E. Lines for the Optimization of the ICP Source Working Conditions

The 71 most sensitive analytical lines of R.E.E. were chosen from tables[17 - 21] and were tested with the aim to select optimum lines for the analysis of R.E.E. ores and mixtures. During the selection, the limits of detection and spectral interferences were considered (cf. Table I). The sums of the first ionization and excitation potentials ($V_{i(1)} + V_{exc}$) of such lines are between 8.3 and 10 V, exceptionally reach 12 V

(ref.[24]). On the basis of values of $V_{i(1)} + V_{exc}$ 4 ionic lines were selected for the optimization (cf. Table II). Atomic lines of R.E.E. are weak and yield high detection limits. However, the axial intensity distributions of both atomic and ionic lines (Y I 410.238 nm was employed) are required to identify particular plasma zones.

Plasma Zones and Spatial Intensity Distributions

The analytical channel of the ICP, surrounded by the induction region (IR), consists of the preheating zone (PHZ), initial radiation zone (IRZ), normal analytical zone (NAZ) and tailflame (T)[25,26]. An axial intensity distribution along the axis of the discharge symmetry (along the channel) and a radial intensity distribution are being distinguished. A lateral intensity distribution observed perpendicularly to the analytical channel is an integral of the radial intensity distribution over the depth of the source along the direction of observa-

TABLE I
Wavelength (nm) of the investigated analytical lines of R.E.E.

La II	Ce II	Pr II	Nd II	Sm II
408.672	446.021	422.533	430.358	443.432
407.735	418.660	422.298	417.732	443.389
366.575	413.765	417.942	415.608	442.434
398.852	413.380	414.341	406.109	428.079
379.478	394.275	400.871	401.225	359.260
379.083	394.215	390.843		
Eu II	**Gd II**	**Tb II**	**Dy II**	**Ho II**
420.505	364.620	387.417	364.541	345.600
412.970	342.247	384.873	353.170	335.898
393.048	336.223	370.392	340.780	
390.710	335.862	370.286		
381.967	335.047	367.635		
		356.852		
		356.174		
		350.917		
Er II	**Tm II**	**Yb II**	**Lu II**	**Y II**
390.634	376.191	369.416	219.139	371.030
349.910	376.133	328.937	261.542	361.105
337.271	370.136	297.056		360.073
	370.026	289.138		
	346.220			
	342.508			
	313.126			

tion. With our equipment, a laterally unresolved emission is measured originating from the horizontal discharge sections of 4 mm height and confined by the aperture. Applying a 4 mm step along the axis we obtain an axial intensity distribution.

Method of Optimization of Operating Conditions

The relaxation method was employed for the optimization. The power input P, outer plasma gas flow rate F_p, intermediate plasma gas flow rate F_a, carrier gas flow rate F_c and the employed observation height h essentially influence the values of *BEC*, I_L and interferences. The maximum net line intensity value I_L, the minimum *BEC* and corresponding values of h and F_c were found for each of the five representative lines listed in Table II. Compromise values of F_c and h were estimated from diagrams for a set of these lines.

Subsequent optimization studies were performed with only two lines representing either extreme F_c or in sums of excitation and ionisation potentials.

Axial intensity distributions of I_L and I_B were then measured for several values of F_p, F_a and P at selected values of F_c, and optimum working conditions for the multielement simultaneous analysis in pure solutions were found. Optimum F_c and h were then found for solutions containing alkali salts or free acids in order to minimize the matrix effect of components coming from the decomposition of samples. The last stage of optimization consisted of selecting analytical lines with minimum spectral interferences under optimum working conditions for simultaneous multielement analysis.

Studies of Spectral Interferences

Respecting the SBW of the spectrometer used (0.03 nm) several types of interference were distinguished from wavelength differences $\Delta\lambda$ between the analytical and interfering lines: (i) $\Delta\lambda \leq 0.005$ nm – true spectral coincidence unresolvable by any spectral instrument due to the physical width of lines emitted by ICP, (ii) $0.005 < \Delta\lambda \leq 0.015$ nm – line overlap unresolvable with SBW = 0.03 nm. A magnitude of the spectral interference strongly depends on the precision of the wavelength adjustment of the movable detector, a monochromator or slits of the polychromator, (iii) $0.015 < \Delta\lambda \leq 0.030$ nm – wing overlap, (iv) $\Delta\lambda > 0.030$ nm – a partial wing overlap with a distant intensive line, or collisionally broadened line. This case also comprises background shifts not attributed to any certain line.

TABLE II

Analytical lines selected for optimization of working conditions of ICP source: V_{exc} excitation potential; $V_{i(1)}$ 1st ionization potential

Line, band nm		V_{exc} V	$V_{i(1)}$ V	$V_{exc} + V_{i(1)}$ V
Nd II	430.358	2.88	5.45	8.33
Gd II	335.862	3.72	6.16	9.88
Lu II	291.139	6.02	6.15	12.17
Y II	371.030	3.52	6.51	10.03
Y II	410.238	3.08	6.51	–
YO II	597.2		7.31[a]	–

[a] Dissociation energy (eV).

Spectra in the vicinity of selected analytical lines were scanned (i) for solutions of particular elements in concentrations between 0.1 and 5 mg l^{-1}, depending on the *BEC* values, (ii) in the presence of interfering R.E.E. at concentrations between 10 to 1 000 mg l^{-1}, (iii) for solutions of a blank containing 0.14 mol l^{-1} HNO_3, (iv) for solutions of accompanying matrix elements, 100 – 1 000 mg l^{-1} Ca, Mg, Sr, Ba, Al, Ti, Fe, Th, Zr, Zn, Cu, Cr, Mo, W and V.

Each interference was characterized by the interference factor a_{ij} which resulted from intensity peak heights according to the expression

$$a_{ij} = (I_{ij}/c_i)/(I_j/c_j) = S_{ij}/S_j , \qquad (4)$$

where S_{ij} and I_{ij} are sensitivity and intensity of the interfering line of the i-th interferent, respectively, at the wavelength corresponding to the maximum of the analytical line of the j-th analyte, S_j and I_j are the sensitivity and intensity of the analytical line of the j-th analyte respectively, and c_j, c_i are the corresponding concentrations. Thus, factor a_{ij} represents the apparent analyte concentration corresponding to a signal of 1 mg l^{-1} of the i-th interferent, measured at the analytical line of the j-th analyte. The 100 a_{ij} value gives directly the percentual relative magnitude of the interference. This format was also used in the computation program for correction of spectral interferences based on solution of a set of linear equations by modified Gauss–Jordan elimination procedure and for calculation of corrected (true) analytical concentrations of R.E.E., assuming that the magnitude of an interfering signal at the particular wavelength of an analytical line is a linear function of an interferent concentration. Algorithms were described in refs[10,13,27]. Checking of the selected factors was performed occasionally using test solutions, in order to assure the accuracy of the mathematic corrections.

The following expression was derived in ref.[28] for the relative standard deviation (RSD) of the corrected concentration c_j, i.e. for s_{rj}

$$s_{rj} = [s_r^2 (1 + 2c_{jb}^2/c_j^2) + 2\sum_{i=1}^{n} (s_r^2 + s_{ra}^2) c_i^2 a_{ij}^2/c_j^2]^{0.5} , \qquad (5)$$

where s_r is the RSD characterizing the stability of the discharge (i.e. the proportionality factor of the flicker noise, cf. refs[29,30]), c_{jb} is the *BEC* value for the j-th analyte's line, a_{ij} is a correction factor, s_{ra} is the RSD of the correction factor a_{ij}, c_j and c_i are the analyte and the interferent concentrations, respectively, and n is a number of interferents. A limit of determination c_D is the concentration determined with the relative standard deviation of concentration s_{rD} equal to 10%. The value c_D is given by the following expression

$$c_D = 2\{[s_r^2 c_{jb}^2 + \sum_{i=1}^{n} (s_r^2 + s_{ra}^2) c_i^2 a_{ij}^2]/(s_{rD}^2 - s_r^2)\}^{0.5} , \qquad (6)$$

where s_{rD} is substituted with the value 0.10, (ref.[28]).

Sample Decomposition

Ore samples, hydroxide and oxidic concentrates were decomposed in dilute HNO_3 (1 : 2, v/v). The insoluble residue of each was fused with Na_2CO_3 or the mixture of Na_2CO_3 and $Na_4B_2O_7$ or with $LiBO_2$. Ores containing high contents of Ba (e.g. 17 wt.% BaO) were fused first with Na_2CO_3, leached with water and the residue on a filter was then dissolved in concentrated HNO_3. Alkaline and acidic solutions were analyzed separately to prevent the precipitation of $BaSO_4$. If the residue on a filter was not dissolved completely

in HNO_3, HBr was added and the solution was combined with the main solution[14]. This residue was proved to consist mainly of a resistant modification of CeO_2 (ref.[14]).

RESULTS AND DISCUSSION

Influence of the Carrier Gas Flow Rate F_c on Axial Distributions of Net Line Intensities I_L for Pure Solutions

The following results from the axial distribution of ionic line intensities compared with the sums of the first ionization and excitation potentials (cf. Table II, Figs 1, 2): (i) the maxima of normalized axial intensity distributions are shifted to higher observation heights with increasing F_c, (Table III), (ii) the I_L vs F_c plots exhibit maxima for all observation heights and are at lower values of F_c for lines with higher values of the sum of $V_{i(1)} + V_{exc}$ (cf. Table III), (iii) observation heights of maxima of axial line intensity distributions for Nd II 430.358 nm, Gd II 335.862 nm and Lu II 291.136 nm decrease with the increasing value of $V_{i(1)} + V_{exc}$ (cf. Tables II, III), (iv) the differences Δh_{max} between observation heights of maximum I_L of the ionic lines decrease with increasing F_c up to 1.3 l min^{-1} Ar but the sequence of maxima remains unchanged between 0.8 – 1.3 l min^{-1} Ar (cf. Table IV), (v) widths of axial intensity distributions I_L^n measured at their half maxima decrease with the increasing F_c, as well as with the increasing value of $V_{i(1)} + V_{exc}$.

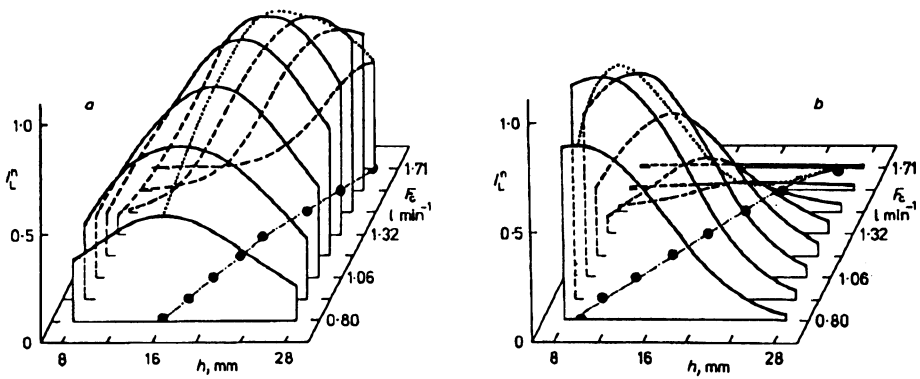

FIG. 1

Dependence of axial intensity distributions of Nd II 430.358 nm (*a*) and Y II 371.030 nm (*b*) on F_c. Intensities are normalized considering the maximum value that corresponds with F_c = 0.8 – 1.9 l min^{-1}, F_a = 0.43 l min^{-1}, F_p = 18.3 l min^{-1}, P = 1.2 kW. Dot line: the shift of the maximum of the distribution with F_c. Dot-and-dash line: the dot line projection into the plane $F_c - h$

The dependence of the observation height of maxima of axial distributions of I_L on the value of $V_{i(1)} + V_{exc}$ is opposite to that for 27.12 MHz ICP, published elsewhere[31 - 35]. Such difference can be explained by different temperature distributions of 27.12 MHz ICP[31 - 34] and 50 MHz ICP sources[21].

Atomic lines of R.E.E. are weak enough in comparison to ionic lines as it is apparent from *BEC* values of Y II 371.030 nm (0.02 mg l^{-1}) and Y I 410.238 nm (8 mg l^{-1}). Similarly, a solution containing 1 000 mg l^{-1} Y is needed in order to achieve measurable intensity of molecular bands of monoxides, such as YO 597.2 nm. In these cases: (i) the minimum of band emission YO 597.2 nm shifts to higher observation height with the increasing F_c. This is caused by the increase of the linear velocity of gas and

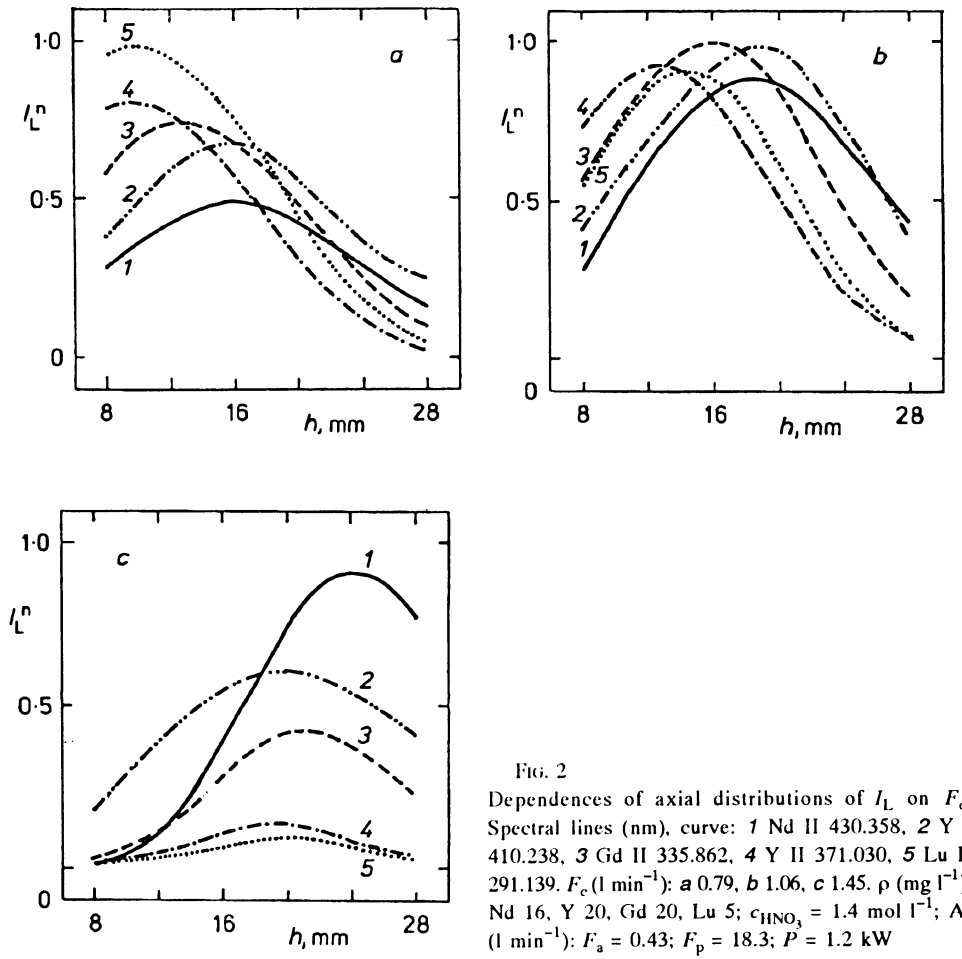

FIG. 2

Dependences of axial distributions of I_L on F_c. Spectral lines (nm), curve: *1* Nd II 430.358, *2* Y I 410.238, *3* Gd II 335.862, *4* Y II 371.030, *5* Lu II 291.139. F_c (l min^{-1}): *a* 0.79, *b* 1.06, *c* 1.45. ρ (mg l^{-1}): Nd 16, Y 20, Gd 20, Lu 5; c_{HNO_3} = 1.4 mol l^{-1}; Ar (l min^{-1}): F_a = 0.43; F_p = 18.3; P = 1.2 kW

TABLE III

Observation heights of maxima of axial intensity distributions of selected lines, h_{max}, and normalized values[a] $I_L^n(h)$ (%), for selected values of F_c

Line, nm		F_c, l min^{-1} Ar							
		0.79	1.06	1.45	0.79	1.06	1.45	1.06	1.45
		h_{max}, mm			I_L^n(max)			I_L^n(16)	I_L^n(20)
Nd II	430.358	16	19	24	50	88	90	83	74
Y II	410.238	16	19	20	67	98	60	92	60
Gd II	335.862	13	16	21	74	100	42	100	42
Y II	371.030	11	13	19	80	92	14	83	14
Lu II	291.139	10	14	20	97	90	9	88	9

[a] Normalized at h_{max} , 16 mm, and 20 mm, respectively; normalization is performed for each line individually and normalized values (%) are related to the highest I_L obtained within the intervals of F_c from 0.7 to 1.9 l min^{-1} and h from 8 to 28 mm. P = 1.2 kW, F_a = 0.43 l min^{-1}, F_p = 18.3 l min^{-1}.

TABLE IV

Dependence of the difference of the maxima heights Δh_{max} (mm)[a] of axial intensity distributions on F_c

Line symbols	F_c, l min^{-1} Ar								
	0.79	0.92	1.06	1.19	1.32	1.45	1.58	1.71	1.85
Nd II – Y I	0	0.4	0.7	1.0	1.4	4.2	8.0	10.0	–
Nd – Y II	8.0	6.7	6.2	5.4	4.6	5.4	4.0	4.0	–
Nd II – Lu II	6.0	5.0	4.5	3.9	3.6	4.3	4.0	–	–
Nd II – Gd II	2.8	3.2	3.7	2.9	2.9	3.6	2.2	4.0	–
Gd II – Y II	5.4	3.5	2.5	2.5	1.7	1.8	1.8	0	–
Y II – Y I	-8.0	-6.5	-5.5	-4.4	-3.2	-1.2	4.0	6.0	15
Lu II – Y II	2.0	1.7	1.8	1.5	1.0	1.1	0	–	–

[a] The difference Δh_{max} of maxima of axial distributions I_L is calculated in the order of line symbols, as they are presented in the 1st column of the table. Negative sign means that the order of positions of maxima relative to the coil is changed. P = 1.2 kW, F_a = 0.43 l min^{-1}, F_p = 18.3 l min^{-1}.

sample, so that the decomposition of YO species occurs higher in the discharge. (ii) The width of the minimum of the axial intensity distribution for YO 597.2 nm decreases with increasing F_c. This corresponds with a contraction of the area of the effective excitation of ionic lines with increasing F_c (Figs 3*a*, 3*b*). (iii) The temperature decrease with increasing h (ref.[21]) above the NAZ stimulates the atomic emission of Y I 410.238 nm and the decrease of ionic emission (Fig. 3*a*) in contrast to the NAZ where 98.7% of atoms are ionized to the 1st degree[36]. Simultaneously, with the decrease of the emission at Y I 410.238 nm by increasing h, the emission of YO 597.2 nm increases (Fig. 3*a*). This agrees with the possible decrease of the concentration of neutral yttrium atoms due to their recombination with oxygen. Moreover, for F_c above 1.3 – 1.4 l min^{-1} the atomic emission at Y I 410.238 nm also decreases because of the cooling effect (Fig. 2*c*). (iv) The maximum of the atomic emission of Y I 410.238 nm is at the same or even higher level above the load coil as those of ionic lines for $F_c \leq 1.3$ l min^{-1} (Figs 2*a*, 2*b* and 3*a*, Tables III, IV) which represents a fundamental difference in comparison with observations of other authors using 27.12 MHz ICP[32,33]. This is probably due to different axial temperature distribution in the analytical channel of 50 MHz ICP[21], since higher oscillator frequencies cause a lower temperature and concentration of electrons[21]. Hence, recombination reactions of Y^+ ions are more significant and atomic lines are more outstanding in the NAZ of 50 MHz ICP than in the usual 27.12 MHz ICPs. For F_c above 1.1 l min^{-1}, the IRZ shifts in the direction of the argon flow (cf. Fig. 3*b*). However, no other maximum of intensity distribution was observed in this area. A

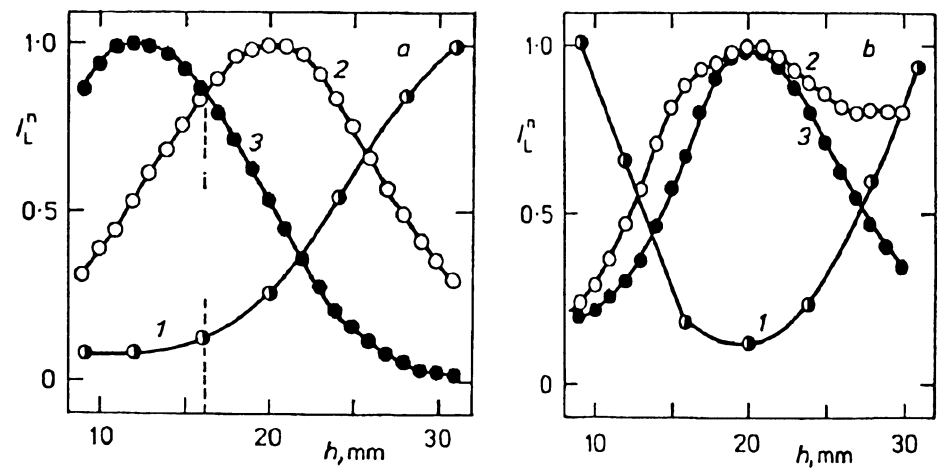

FIG. 3

Axial distributions of normalized intensities I_L^n for F_c = 1.06 (*a*) or 1.45 l min^{-1} (*b*); curve: *1* YO 597.2 nm, *2* Y I 410.238 nm, *3* Y II 371.030 nm. Normalization of I_L for each line individually against the maximum value for F_c = 1.06 l min^{-1} (*a*) and F_c = 1.45 l min^{-1} (*b*). Ar (l min^{-1}): F_a = 0.43, F_p = 18.3; P = 1.2 kW; i internal reference point

common position of maxima of atomic and ionic intensity distribution, as well as the minimum on the molecular emission distribution plot (Fig. 3*b*) proves the maximum temperature in the NAZ at h = 20 mm and the high flow rate F_c = 1.45 l min^{-1}. For high F_c (F_c > 1.5 l min^{-1}) the ionic line intensity distribution plots had their maxima at higher observation heights than the emission distribution of atomic lines (compare Y II 371.030 nm with Y I 410.238 nm and Table IV) but the emission intensity was too weak under such conditions and not suitable for analytical purposes. Doubled maxima of axial intensity distribution could not be proved by our measurement at Y I 410.238 nm. This is in disagreement with references where doubled maxima on intensity distribution plots were mentioned[36 - 38]. A comparison between axial distributions of ionic and atomic lines of yttrium of various origin is based on Table V (refs[36,38]) and corresponding operation conditions from Table VI. Thus, at relatively close ICP opera-

TABLE V
Comparison of observation heights h_{max} of maxima of axial intensity distributions of Y II and Y I lines, observation heights of intersections h_x of these distributions, and observation heights h_o of boundary IRZ/NAZ for experimental conditions presented in Table VI

Spectral line nm		V_{exc} V	$V_{exc} + V_{i(1)}$ V	h_{max} mm		h_x mm	h_o[b] mm	Ref.
Y I	Y II	Y I	Y II	Y I	Y II			
296.5	298.1	4.25	14.21	6.5	13.0	8.0	9.0	36
296.5	317.9	4.25	10.53	6.5	13.0	8.0	9.0	36
407.7	371.0	3.04	10.03	10	17	12.6	13.0	38
410.2	371.0	3.08	10.03	18.0	12.5	15.2	8 – 9[a]	[c]
410.2	371.0	3.08	10.03	20.0	12.0	16.2	8.5	[c]

[a] Height of the observation zone 4 mm, in other cases 1 mm; [b] YO 597 nm; [c] this work.

TABLE VI
Working conditions for comparing ICP sources

f, MHz	P, kW	F_p, l min^{-1}	F_a, l min^{-1}	F_c, l min^{-1}	Ref.
27.12	1.25	16	0.8	0.45	38
27.12	1.1	16	1.0	1.0	36
50	1.2	18.3	0.43	1.06	[a]

[a] This work.

ting conditions except the generator frequency the maxima of ionic emission of yttrium are observed coincidently at 12 – 13 mm above the load coil while the maximum of atomic emission of yttrium is observed by 6 – 7 mm lower for 27.12 MHz and by 6 – 8 mm higher for 50 MHz ICP than the maxima of ionic emission distributions.

Comparing our results for 50 MHz ICP with the results of other authors shows that the atomic emission in the NAZ of 50 MHz ICP is more conspicuous than in the NAZ of 27.12 MHz ICP. Moreover, more significant differences between axial intensity distributions of various ionic lines exist in the NAZ of 50 MHz ICP. Respecting the axial intensity distributions of ionic lines, compromise conditions were selected to reach simultaneously the optimum intensity of each of those lines (cf. Table III). Thus, the values of F_c = 1.06 l min^{-1} and h = 16 mm at F_p = 18.3 l min^{-1}, F_a = 0.43 l min^{-1} and P = 1.2 kW can be regarded as compromise conditions for multielement analysis to reach maximum sensitivity of the calibration plot.

Influence of F_c on Axial Distribution of Background Intensities I_B and BEC for Pure Solutions

For ionic lines Nd II 430.358 nm, Y II 371.030 nm and Gd II 335.862 nm the background emission is formed by the recombination continuum of Ar^+ and hence, the background intensity decreases with increasing h and F_c. On the other hand, the molecular emission of NH species (λ_{max} = 366.0 nm) contributes to the background emission of the line Gd II 335.862 nm (Fig. 4). As the temperature of the plasma decreases with increasing h and F_c, the recombination degree of NH molecules increases and an increased background is observed at h > 16 mm (Fig. 4).

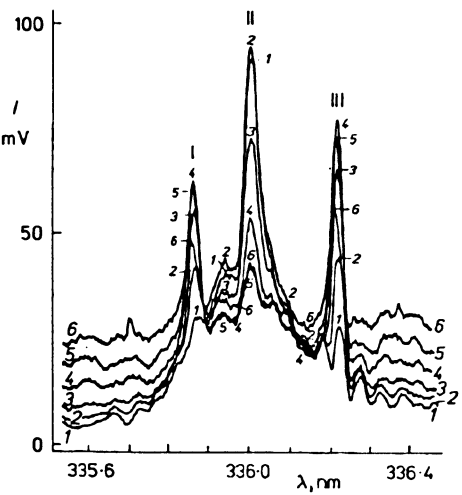

FIG. 4

Spectrum of the band NII 336.0 nm at various observation heights in the presence of 2 mg l^{-1} Gd. h (mm): *1* 28, *2* 24, *3* 20, *4* 16, *5* 12, *6* 8. I Gd II 335.862 nm, II NII 336.0 nm, III Gd II 336.2233 nm. F_c = 1.06 l min^{-1}; Ar (l min^{-1}): F_a = 0.43, F_p = 18.3;

Concerning *BEC*, different courses versus the observation heights were observed. If the decrease of background intensity is steeper with the increasing h than the decrease of the line intensity, the resulting value of *BEC* decreases with the increasing h continuously (e.g. for line Nd II 430.358 nm, Fig. 5*a*). In the opposite case, the plot of *BEC* against h exhibits a minimum (line Lu II 291.139 nm Fig. 5*b*). For the line Gd II 335.862 nm, the background intensity is composed of the argon recombination continuum and the molecular band emission NH 336.0 nm. It decreases less than the particular line intensity with increasing h which awoke a minimum on the axial distribution of *BEC*. Taking into consideration the above compromise conditions for optimum sensitivity, satisfactorily low values of *BEC* were reached for observation heights between 16 – 20 nm and F_c between 0.9 – 1.3 l min^{-1}.

Influence of the Outer and Intermediate Gas Flow Rates F_p, F_a on the Line and Background Intensities and BEC

For typical lines Nd II 430.358 nm and Y II 371.030 nm, the axial distributions of their I_L, I_B and *BEC* are very similar for F_p between 15.0 and 21.6 l min^{-1}, in spite of different excitation energies (Figs 6*a*, 6*b*). As I_B^n increases more significantly than I_L^n, *BEC* increases within the whole range of axial distribution and the range of studied h (Fig. 6*c*).

On the other hand, intensities of the line Nd II 430.358 nm and Y II 371.030 nm reached their maximum values for F_a = 0.43 l min^{-1} (Figs 7*a*, 7*b*). The bottom of the discharge removes from the injector orifice at the increasing F_a. At $F_a \approx 2.5$ l min^{-1}, the

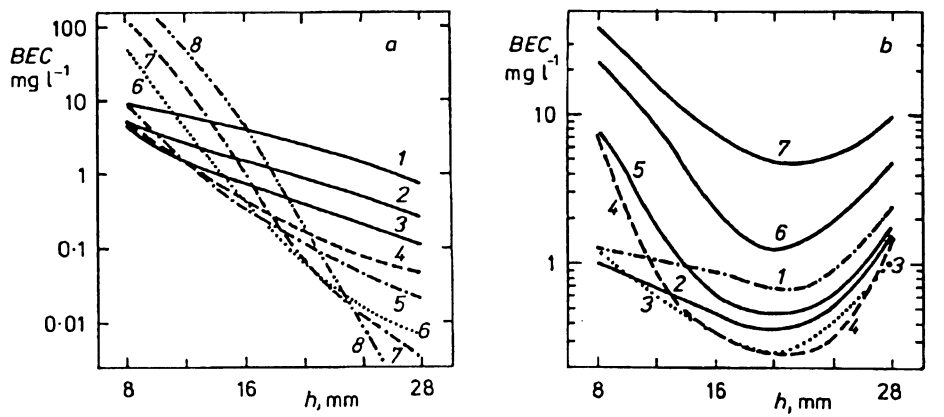

FIG. 5
Axial distribution of *BEC* for Nd II 430.358 nm (*a*) and Lu II 291.139 nm (*b*). F_c (l min^{-1}): *1* 0.79, *2* 0.92, *3* 1.06, *4* 1.19, *5* 1.32, *6* 1.45, *7* 1.58, *8* 1.71. Ar (l min^{-1}): F_a = 0.43, F_p = 18.3; P = 1.2 kW

discharge bottom approaches the upper rim of the load coil and the discharge becomes unstable. Reducing F_a towards zero shifts the discharge bottom upstream and the injector orifice and the rim of the intermediate tube are in danger of melting.

For the plasma torch used, the shift of the maximum of the distribution of I_L^n to higher observation heights is connected with the displacement of the discharge bottom (Figs 7*a*, 7*b*). A similar behaviour was observed for F_a = 1.45 l min^{-1}. The intermediate gas flow contributes to the formation of the plasma toroid but a part is probably mixed with the carrier gas. This leads to increased cooling of the analytical channel and consequently to the decrease of the intensity of the line Y II 371.030 nm (Fig. 7*a*). As the line Nd II 430.358 nm has a lower sum of $V_{i(1)} + V_{exc}$ (cf. Table II) than Y II

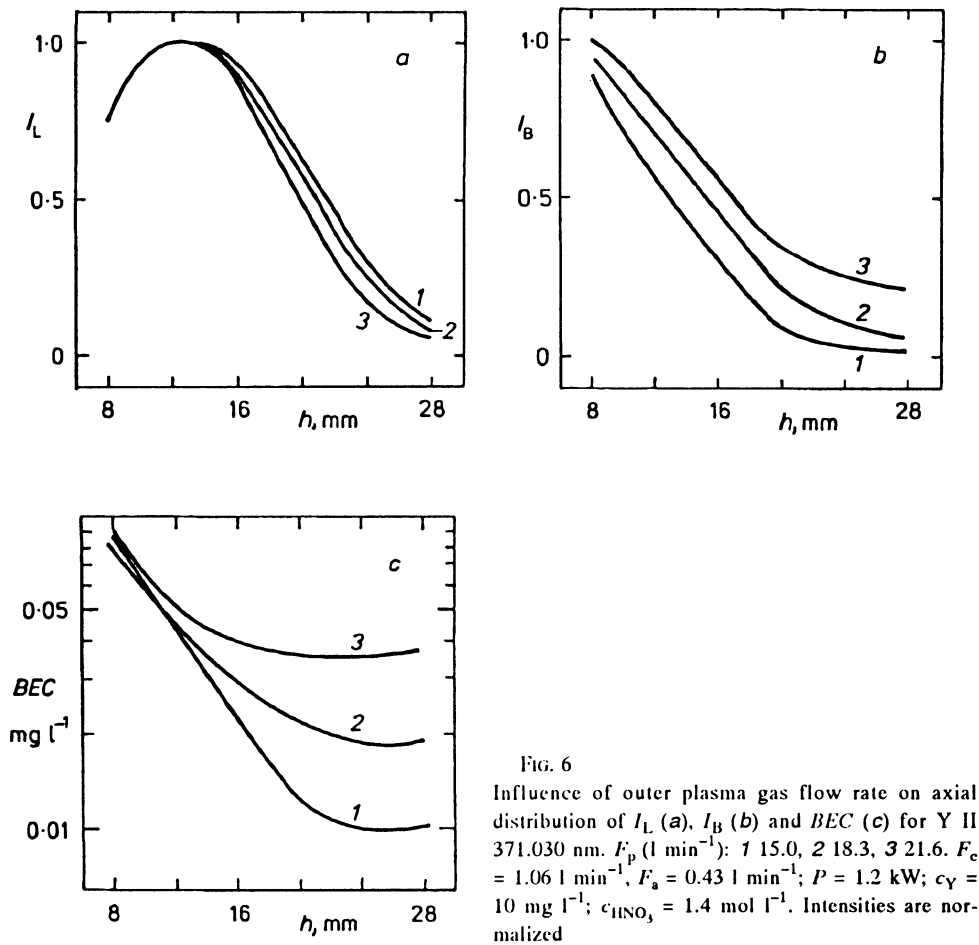

FIG. 6

Influence of outer plasma gas flow rate on axial distribution of I_L (*a*), I_B (*b*) and *BEC* (*c*) for Y II 371.030 nm. F_p (l min^{-1}): *1* 15.0, *2* 18.3, *3* 21.6. F_c = 1.06 l min^{-1}, F_a = 0.43 l min^{-1}; P = 1.2 kW; c_Y = 10 mg l^{-1}; c_{HNO_3} = 1.4 mol l^{-1}. Intensities are normalized

371.030 nm, the cooling effect does not occur for F_c = 1.06 l min^{-1} (Fig. 7*b*) in contrast to F_c = 1.45 l min^{-1}. The cooling effect is apparent on the behaviour of I_B (Fig. 7*c*). On the other hand the corresponding *BEC* values do not change essentially with F_a. Therefore, it is convenient for analytical purposes to apply the lowest intermediate gas flow level which ensures the necessary gap between the rim of the intermediate tube and the discharge bottom.

Influence of the Power Input P on Axial Intensity Distributions and BEC Values for Pure Solutions

At F_c between 0.8 and 1.5 l min^{-1} and P between 1.2 and 1.6 kW, both the line and background intensities are enhanced with the increase of P and the positions of maxima

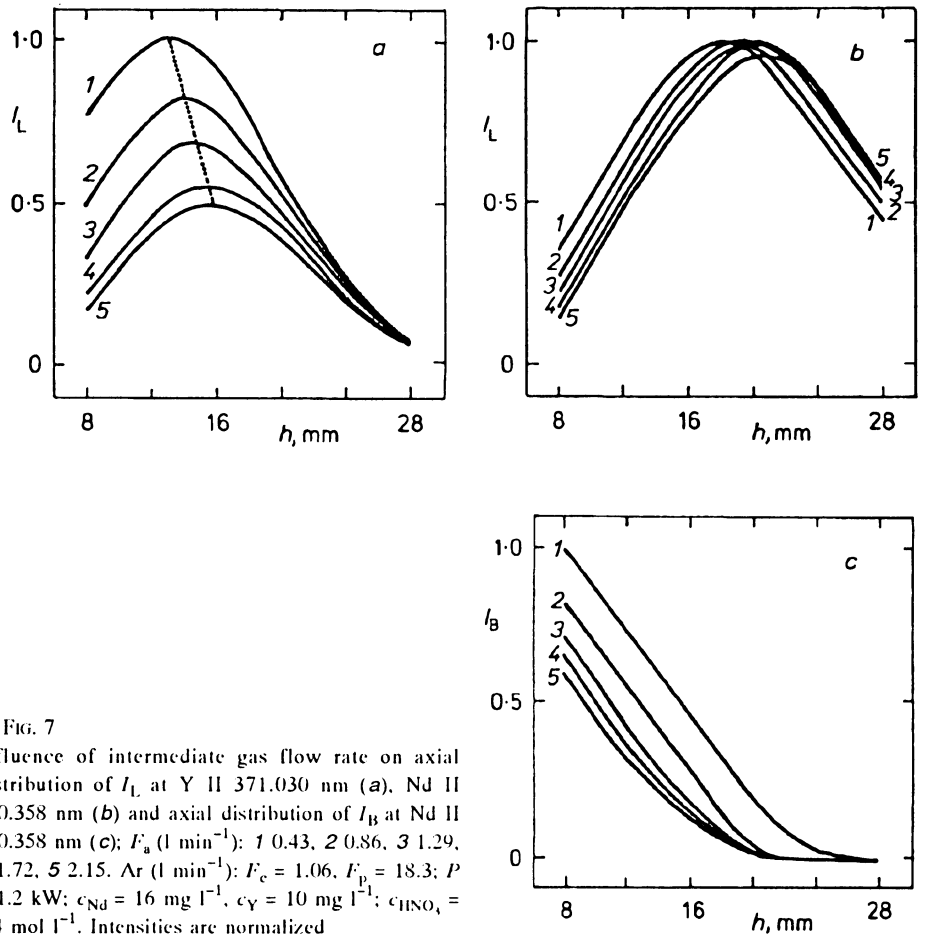

FIG. 7
Influence of intermediate gas flow rate on axial distribution of I_L at Y II 371.030 nm (*a*), Nd II 430.358 nm (*b*) and axial distribution of I_B at Nd II 430.358 nm (*c*); F_a (l min^{-1}): *1* 0.43, *2* 0.86, *3* 1.29, *4* 1.72, *5* 2.15. Ar (l min^{-1}): F_c = 1.06, F_p = 18.3; P = 1.2 kW; c_{Nd} = 16 mg l^{-1}, c_Y = 10 mg l^{-1}; c_{HNO_3} = 1.4 mol l^{-1}. Intensities are normalized

of axial distributions of I_L are shifted. This enhancement is more significant for Y II 371.030 nm than for Nd II 430.358 nm. The cooling effect of F_c is therefore more significant for the yttrium line at increasing P. As *BEC* also rises for both the tested lines with the increasing P, the lowest P value ensuring a stable operation of the discharge (i.e. P = 1.2 kW) was further used with F_p = 18.3 l min^{-1}, F_a = 0.43 l min^{-1} and F_c = 1.06 l min^{-1}.

Evaluation of the Internal Reference Point (IRP) in the ICP

The IRP serving for a quick indentification of the NAZ[25,36,38,39] was evaluated as the intersection of normalized axial intensity distributions of atomic and ionic lines of yttrium (Y II 371.030 nm and Y I 410.238 nm) (cf. Fig. 3*a*). Maintaining the optimum values of P, F_p and F_a for pure solutions and F_c = 0.9 – 1.3 l min^{-1} the observation height h_x of the IRP is practically identical with the optimum observation height for the particular F_c (compare the optimum height of 16 mm from Table III with the value of $h_x \approx 15 - 16$ mm from Table V).

According to refs[36,38], the observation height h_x corresponding to the intersection of intensity distributions of atomic and ionic yttrium lines is identical with h_o of the boundary between the NAZ and the IRZ characterized by the emission of molecules of YO (cf. Table V). The optimum observation height is reported to be approximately 5 mm above this boundary or IRP, respectively[38]. In our case of 50 MHz ICP, the IRP is placed some 7 – 8 mm above the boundary of the IRZ and the NAZ. These differences between 27.12 MHz and 50 MHz ICPs result from their opposite sequences of axial intensity distributions of ionic and atomic lines against the load coil.

Matrix Interferences of Salts of Alkali Metals

The axial distribution of the matrix effect X was studied on intensities I_L of model lines Nd II 430.358 nm, Y II 371.030 nm and Y I 410.238 nm for F_a = 0.43 l min^{-1}, F_c = 18.3 l min^{-1}, P = 1.2 kW and the carrier gas flow rate interval F_c = 0.8 – 1.9 l min^{-1} (Fig. 8). In the presence of 0.1 mol l^{-1} $NaNO_3$: (i) a decrease of I_L of ionic lines by 5 – 15% in comparison with pure solutions for the observation height interval between 8 – 28 mm and F_c = 0.8 – 1 l min^{-1} is observed (Figs 8*a*, 8*c*). The depression of atomic line takes place in the range of h between 8 and 24 mm which can be considered as the NAZ. Above this height, an enhancement of the line intensity is observed (Fig. 8*b*) because the ionization equilibrium of yttrium is influenced; (ii) the depression of I_L of all lines in the NAZ is practically independent of h and changes only little for F_c between 0.8 – 1.0 l min^{-1} (Fig. 8*c*); (iii) for F_c > 1 l min^{-1}, the intensity I_L of the ionic lines is enhanced above h = 8 mm. Using larger F_c, the interval of increased I_L shifts downstream. For particular carrier gas flow rate, the area of enhanced intensity of Y II 371.030 nm reaches higher observation height than the emission area of YO 597.2 nm, at

least by 5 mm (cf. Fig. 8). This means that the IRZ, characterized by the area of the enhanced intensity of Y II 371.030 nm in the presence of easily ionizable elements is closer to the internal reference point than when characterized by the area of band

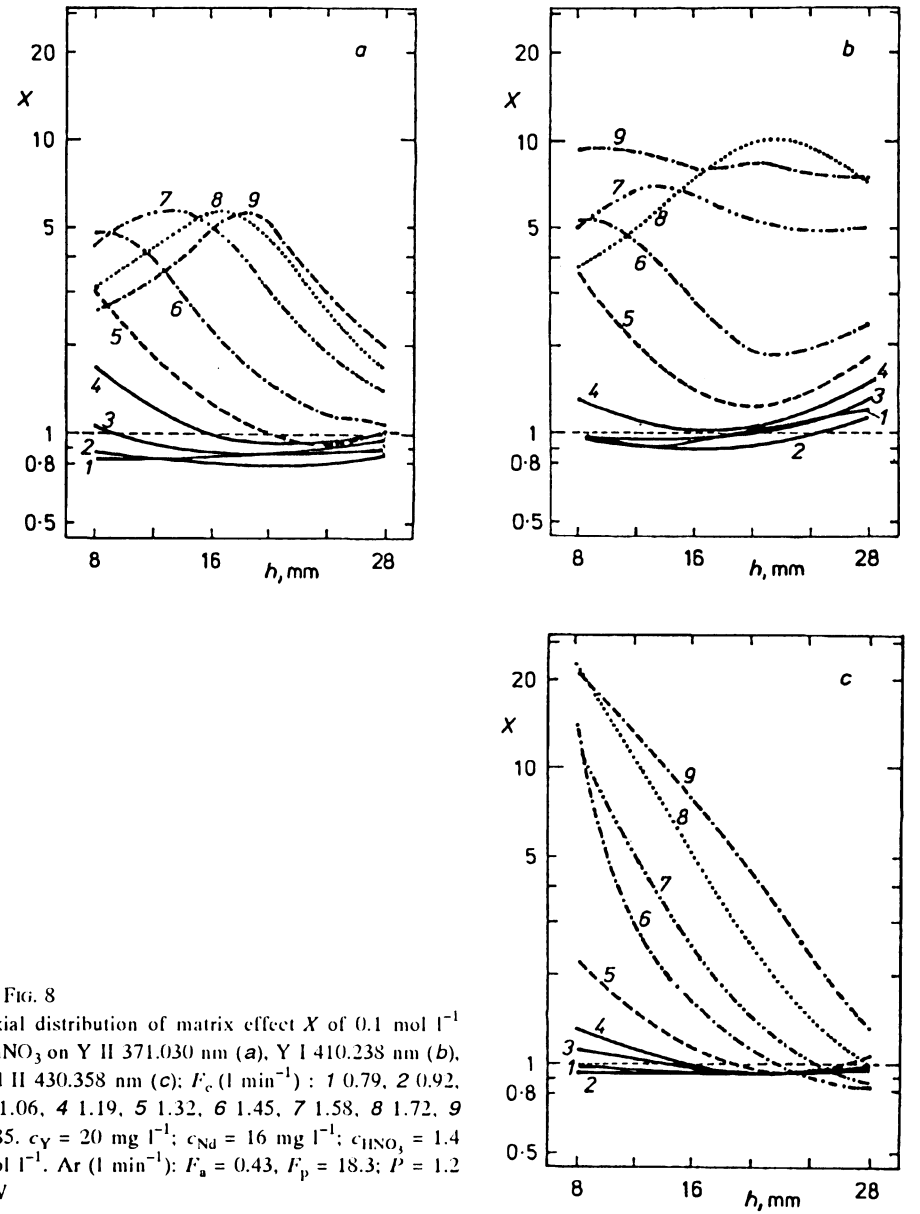

FIG. 8

Axial distribution of matrix effect X of 0.1 mol l^{-1} $NaNO_3$ on Y II 371.030 nm (*a*), Y I 410.238 nm (*b*), Nd II 430.358 nm (*c*); F_c (l min^{-1}) : *1* 0.79, *2* 0.92, *3* 1.06, *4* 1.19, *5* 1.32, *6* 1.45, *7* 1.58, *8* 1.72, *9* 1.85. c_Y = 20 mg l^{-1}; c_{Nd} = 16 mg l^{-1}; c_{HNO_3} = 1.4 mol l^{-1}. Ar (l min^{-1}): F_a = 0.43, F_p = 18.3; P = 1.2 kW

emission YO 597.2 nm. (iv) The simultaneous increase of atomic and ionic line intensities of yttrium in the IRZ gives evidence of the collisional excitation by electrons rather than of the influenced ionization equilibrium of yttrium; (v) for the increased value of $F_c \leq 1.4$ l min^{-1} (curves *4 – 6* in Figs 8*a*, 8*c*) the course of the intensity enhancement of both ionic lines is practically the same; (vi) differences in axial distributions of the matrix effect X on both ionic lines above $F_c > 1.4$ l min^{-1} can be explained by different "hardness"[22] of these lines.

The increase of atomic emission at height h above 24 mm (tailflame area, refs[25,39]) is probably caused by a decrease of ionization degree of yttrium due to the increased concentration of electrons from the ionized sodium atoms. The assumed concentration of electrons from the ionization of argon in the plasma is about $1 . 10^{14}$ or $2 . 10^{14}$ cm^{-3} at h above 25 mm (ref. [40]). About $1 . 10^{14}$ cm^{-3} electrons are released from complete ionization of 0.1 mol l^{-1} Na which influence the ionization equilibrium of yttrium. The electron temperature is lower at this observation height than in the NAZ and the IRZ. Thus, the recombination reaction is probable:

$$M^+ + e^- \longrightarrow M + h\nu_c \qquad (7)$$

or the excitation:

$$M + e_1^- \longrightarrow M^* + e_2^-, \qquad (8)$$

where M^+, M belong to the analyte, indices 1 and 2 denote different kinetic energies of electrons and $h\nu_c$ the energy of continuous recombination radiation. The excited state of the atom is denoted with an asterisk.

The decrease of I_L in the NAZ is due rather to the changes in physical properties of the nebulized solution in the presence of a salt, such as sodium nitrate. Since the concentration of electrons from the ionization of argon is about $1 . 10^{15}$ cm^{-3} in the NAZ[40], the influence of ionization of sodium atoms is less significant for the collisional excitation or the recombination than in the zone of IRZ or in the tailflame.

A course of the axial distribution of the matrix effect X on the line Y II 371.030 nm at F_c above 1.4 l min^{-1} (Fig. 8*a*) probably results from the temperature decrease in the analytical channel with increasing F_c. Thus, the fraction of electrons having increased energy suitable for the excitation of ions:

$$M^+ + e_1^- \longrightarrow M^{+*} + e_2^- \qquad (9)$$

decreases with increasing F_c. Therefore, the enhancement of the matrix effect X is not observed at the line Y II 371.030 nm with the large sum $V_{i(1)} + V_{exc}$ for $F_c > 1.4$ l min^{-1} and $h < 16$ mm in contrast to the line Nd II 430.358 nm (Fig. 8*c*). The dissociation of YO is also limited by the temperature decrease, as it can be concluded from the decrease of the emission of the band YO 597.2 nm with increasing F_c (cf. Fig. 3*b*). However,

the main reason is the decrease of temperature of electrons since the dissociation energies of both oxides are very close, namely for NdO (7.02 ± 2) eV and (7.31 ± 0.1) eV for YO, respectively. In spite of that, the same course of axial distribution of interfering effect is not observed.

The decrease of the matrix effect X with increasing h in the IRZ is probably due to the increased concentration of electrons from the ionization of Ar with the increasing h (ref.[41]). Hence, the relative concentration increase of electrons from the ionization of sodium atoms is lower and the influence on collisional excitation also diminishes.

At the same molar concentration of salts of various easily ionisable elements the boundary between the IRZ and NAZ shifts downstream into the plasma with the decreasing ionization potential of the interferent (Figs 9*a*, 9*b*).

At $F_c \geq 1.3$ l min^{-1}, the observation height of the IRZ and the NAZ boundary depends on the analyte, i.e. it shifts downstream with the increasing value of the sum $V_{i(1)} + V_{exc}$ of the analyte.

The dependences of the matrix effect X on the increasing concentration of the alkali metal salts were examined for $LiNO_3$ in the concentration interval 300 – 4 500 mg l^{-1} Li and for $NaNO_3$ in the interval 100 – 9 200 mg l^{-1} Na on the selected lines Y II 371.030 nm and Nd II 430.358 nm. Measurements were performed for F_c between 0.8 – 1.5 l min^{-1} Ar at observation heights 8, 12, 16, 24 and 28 mm. In such cases, plots of X indicate both, depressive and enhancing effect. In the IRZ the plot of X against the concentration of $NaNO_3$ is practically linear in log–log coordinates for both, the Nd-

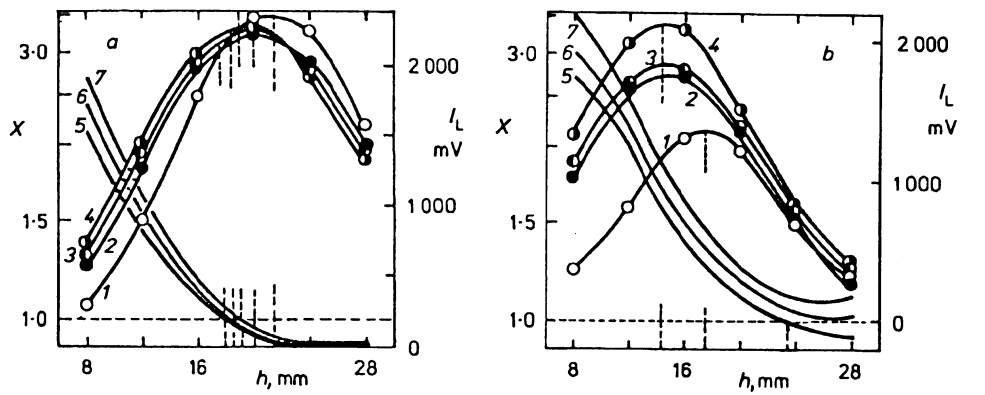

FIG. 9

Influence of Li^+, Na^+ and K^+ ions in solutions on axial intensity distributions of I_L for Nd II 430.358 nm (*a*) and Y II 371.030 nm (*b*). Axial distributions of I_L: *1*, *2*, *3* and *4*. Axial distributions of X : *5*, *6* and *7*. Matrix composition: *1* pure solution; *2*, *5* $LiNO_3$; *3*, *6* $NaNO_3$; *4*, *7* KNO_3. $c_{LiNO_3} = c_{NaNO_3} = c_{KNO_3} = 0.1$ mol l^{-1}; $c_{HNO_3} = 1.4$ mol l^{-1}; $c_{Nd} = 4$ mg l^{-1}; $c_Y = 1$ mg l^{-1}. Ar (l min^{-1}): $F_c = 1.06$, $F_a = 0.43$, $F_p = 18.3$.

and Y- lines, as it is evident from Fig. 10*a*, curve *1* and from Fig. 10*b* curves *1*, *2* (Nd II 430.358 nm). For the NAZ the decrease of X with increasing concentration of $NaNO_3$ is non-linear (Fig. 10*a*, curves *2*, *3*, *4* and Fig. 10*b*, curve *3*). The value of X is constant at the boundary between the channel zones (Fig. 10*b*, curve *3*). In order to eliminate the influence of salts of easily ionizable elements on the net line intensities, the analytical condition must be confined to h = 16 – 20 mm and to F_c = 0.9 – 1.2 l min^{-1} Ar.

Matrix Interferences of Some Other Elements

The effect of various elements was studied in the IRZ and the NAZ. The non-spectral interference of cerium, the main R.E.E. component in some of analyzed samples was investigated on the model lines Y II 371.030 nm and Nd II 430.358 nm. Introducing corrections for spectral interferences prior to matrix effect evaluation, the course of axial intensity distributions for the above lines, as well as that of the resulting matrix effect X are similar to those obtained for easily ionizable elements (e.g. Fig. 9*a*). A similar matrix effect is observed in the presence of 0.012 mol l^{-1} Zn (Fig. 11, curves *2*, *3*) although the first ionization potential of Zn is rather high (9.39 eV). On the other hand, zirconium in 0.011 mol l^{-1} concentration causes depressions at high carrier gas flow rates along the whole axial range (Fig. 11, curves *2'*, *3'*). This depression comes probably from the formation of stable oxidic species of Zr with Nd or Y.

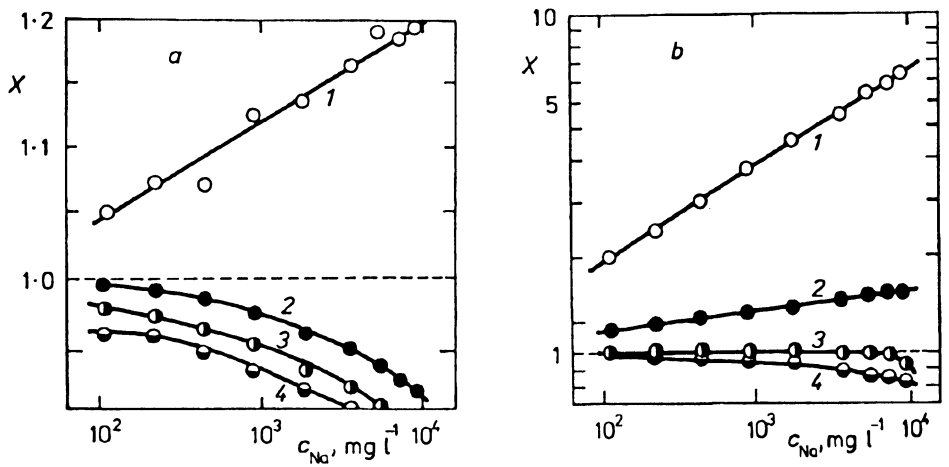

FIG. 10

Dependence of matrix effect X for Nd II 430.358 nm on the concentration of $NaNO_3$. F_c (l min^{-1}): *a* 1.06, *b* 1.45; h (mm): *1* 8, *2* 16, *3* 20, *4* 24. Ar (l min^{-1}): F_p = 18.3, F_a = 0.43; P = 1.2 kW; c_{Nd} = 16 mg l^{-1}; c_{HNO_3} = 1.4 mol l^{-1}

Summarizing, non-spectral interferences occur usually at high carrier flow rates not only in the presence of easily ionizable elements but also in the presence of another R.E.E., in the presence of an element with a high ionization potential and the element forming stable oxidic compounds. At values of F_c (1 – 1.2 l min^{-1} Ar) and observation heights 16 – 20 mm, however, no matrix effects of Ce, Zn, or Zr were observed (see also Fig. 11, curves *1*, *1'*).

Moreover, at compromise conditions of F_c = 1.06 l min^{-1} Ar, h = 16 mm, F_a = 0.43 l min^{-1} Ar, F_p = 18.3 l min^{-1} and P = 1.2 kW, the value X = 0.95 was found for both Y II and Nd II model lines in the presence of 1 000 mg l^{-1} of Ca, Mg, Sr, Ba, Al and Si and 3 000 mg l^{-1} of $LiBO_2$.

Influence of Acids

The influence of strong acids on I_L was examined on model lines Nd II 430.358 nm and Y II 371.030 nm for F_c between 0.8 – 1.5 l min^{-1} Ar and the observation heights between 8 – 24 mm. The net line intensities considerably decrease for both lines with the increasing concentration of HCl. This depression depends on the observation height, especially in the case of more than 4 mol l^{-1} HCl (Fig. 12). Such a dependence was observed on the axial distribution of X, too. Under compromise conditions mentioned before, i.e. F_c = 1.06 l min^{-1} and h = 16 mm, the net line intensity depression is

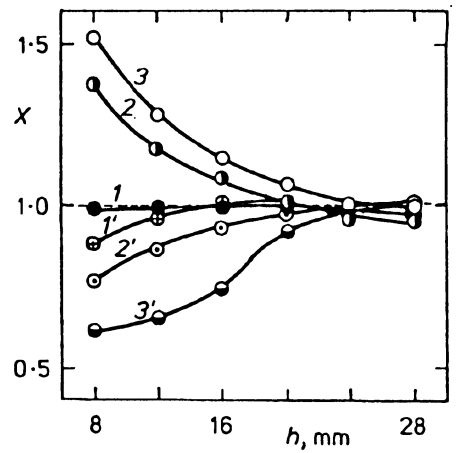

FIG. 11
Axial distribution of matrix effect X of 0.1 mol l^{-1} Zn and Zr on Y II 371.030 nm. Matrix: *1*, *2*, *3* Zn; *1'*, *2'*, *3'* Zr. F_c (l min^{-1}): *1*, *1'* 1.06; *2*, *2'* 1.45; *3*, *3'* 1.72. c_Y = 10 mg l^{-1}; c_{Zn} = 800 mg l^{-1}; c_{Zr} = 1 000 mg l^{-1}; c_{HCl} = 2.0 mol l^{-1}; Ar (l min^{-1}): F_a = 0.43, F_p = 18.3; P = 1.2 kW

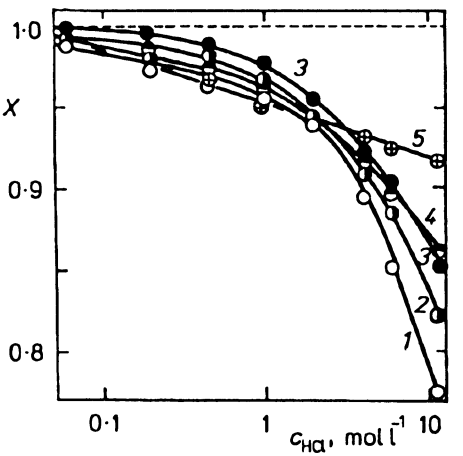

FIG. 12
Dependence of matrix effect X of HCl on the concentration of HCl for Nd II 430.358 nm. h (mm): *1* 8, *2* 12, *3* 16, *4* 20, *5* 24. Ar (l min^{-1}): F_c = 1.06, F_a = 0.43, F_p = 18.3; P = 1.2 kW; c_{Nd} = 16 mg l^{-1}

minimal and X reaches its maximum value. The conspicuous axial distribution of X exhibits its maximum for large F_c = 1.45 l min^{-1} at h = 16 – 17 mm which coincides with the position of the maximum emission of Y II 371.030 nm and Y I 410.238 nm (cf. Fig. 3*b*) and the minimum emission of YO 597.2 nm at this F_c. As considerable changes of the axial distribution plot of I_L and the existence of the maximum on the axial distribution plot of X in the presence of large excess of HCl were observed, excitation processes are probably influenced. On the contrary, at low values of F_c, simple depression occurs only due to the change of nebulisation and transport efficiency. The steepest drop of I_L was observed below 1 mol l^{-1}. Thus, it is recommended to maintain always the same concentration of acid in calibration and sample solutions. Similar concentration plots of I_L were observed with HNO_3, as well as for the background emission.

Concentrations Plots and Precision

The linearity of I_L-plots against concentration was tested for lines with different excitation characteristics and *BEC* values, such as Gd II 336.223 nm and Y I 410.238 nm (high *BEC*) or Y II 371.030 nm and Eu II 381.97 nm (low *BEC*).

For Gd II, the linearity was proved over 3 orders of concentration (0.25 – 100 mg l^{-1} Gd), for Eu II and Y II at least over 4 orders (0.01 – 100 mg l^{-1} Eu, or Y) using compromise optimum conditions, P = 1.2 kW, F_c = 1.06 l min^{-1}Ar, h = 16 mm .

The plots remained linear for atomic and ionic lines in the NAZ even in the presence of the excess of alkaline metals salts. The resulting decrease of the slopes is constant for a particular concentration of the interferent. In the IRZ, deviations from linearity of the plots were observed for pure R.E.E. solutions, as well as and in the presence of interferents.

The precision of measurements for the total intensity of line and corresponding background (I_L + I_B) is characterized by a constant standard deviation (SD) for R.E.E. concentrations lower than the doubled value of *BEC* and by a constant RSD for concentrations higher than this value (e.g. 0.5 – 200 mg l^{-1} for Nd II 430.358 nm) and approximately 0.5% for integration times greater than 10 s. The nebulization and aerosol transport processes are significant sources of noise in our ICP-OES equipment, being influenced by Ar flow fluctuations because no flow mass controller was available. For F_c = 1.06 l min^{-1} Ar, the fluctuations of intensities are characterized by RSD of I_B and I_L 0.6% and 0.4%, respectively. The precision of detectors and the measuring electronics, determined using a stabilized light source, was found to be about 0.2% for integration times greater than 10 s. When the quantizing error (error of reading of low values) was eliminated and its influence on overall precision was distinguished, it was found that a considerable increase of the RSD observed below the 10 s integration time can be attributed mainly to the ICP source. This increase was found to be inversely proportional to the integration time.

Spectral Interferences

The particular number of R.E.E. alternative lines to be tested for spectral interferences depends on the complexity and diversity of samples to be analyzed which are:

a) raw materials of R.E.E. such as Kola-apatite, bastnesite and concentrates of these. Oxides of La, Ce, Pr and Sm form 70 – 99% of the sum of R.E.E. oxides and therefore their spectral interferences are expected predominantly. Such materials also contain Th and Y and common elements such as Ca, Ba, Sr, Mg, Al, Ti, Si and P;

b) lanthanoid concentrates after separation of Ce and La, containing Y. More important are spectral interferences of Pr, Nd and heavier R.E.E.;

c) separated individual oxides of various grades of purity: in these cases the collisional broadening of lines and scattered light from the intensive lines of particular matrix R.E.E. contribute to spectral interferences predominantly;

d) eluted fractions after separation on cation exchangers including those in Zn^{2+} and Cu^{2+} cycle and using NTA or EDTA as mobile phase. Spectral interferences of R.E.E. neighbours with the particular fraction if present in concentration ratios of several orders of magnitude as well as those of Cu and Zn;

e) aqueous phases after solvent–solvent extraction of R.E.E. in the presence of $Ca(NO_3)_2$ excess as salting-out agent. A high level of stray-light from intensive Ca lines is expected.

Spectra were scanned for 71 R.E.E. prominent analytical lines in the presence of interferents. A set of 30 optimum lines was selected, 2 lines for each R.E.E. (cf. Table VII). Attained values of *BEC* are comparable with those in ref.[19].

The magnitude of a_{ij} depends also on the working conditions of the ICP source. The influence of F_c on the axial distribution of factor a_{ij} representing the spectral interference of Yb II 291.152 nm on the model analytical line Lu II 291.139 nm was studied. The minimum factor a_{ij} is obtained for F_c between 1.1 – 1.2 l min^{-1} Ar, maintaining F_p = 18.3 l min^{-1}, F_a = 0.43 l min^{-1} and P = 1.2 kW constant at the optimized h = 16 – 20 mm.

Ionization energies of atoms and ions of the analyte and interferent and excitation energies of both transitions influence mainly the changes of a_{ij} with changing operating conditions of ICP. Results of tests with various analytical lines of the determined R.E.E. in the presence of interfering R.E.E. prove that a_{ij} decreases mostly with the increasing F_c and the observation height[11].

The correction factor a_{ij} expressing the interference of Tb II 353.186 nm with the analytical line Dy II 343.170 nm was used to evaluate the precision, short-term and the long-term repeatabilities of a_{ij}. The precision with the RSD of 1.85% follows from 10 successive measurements and evaluations of the correction factor $a_{ij} = 0.325 \cdot 10^{-2}$. The short-term repeatability within the time interval of 8 h corresponds with the RSD of 5.4% from 10 repetitions. The same solutions for blank, analyte and interferent were used as above. The RSD of a_{ij} was somewhat worse (7.1%) in the presence of 5 000

mg l^{-1} $LiBO_2$. The long-term repeatability found from 10 measurements performed in the course of 4 years with the same plasma torch was characterized by the RSD of 18.4%. During routine measurements the most significant interferences were checked daily and the RSD did not exceed 5 – 10%.

TABLE VII
BEC values and correction factors 100 a_{ij} for optimum analytical lines (ionic, II)

Anal. line	λ nm	*BEC* mg l^{-1}	100 a_{ij}, ppm analyte/100 ppm interferent			
			⟨10; 1⟩	⟨1; 0.5⟩	⟨0.5; 0.1⟩	<0.1
La	408.67	0.29	Th	Sr, Nd, Tb	Pr, Ce, Dy	Sm, Eu, Ho, Er
La	398.85	0.35		Nd, Pr	Eu, Ca, Yb	Th, Sm, Ti, Ho
Ce	413.77	1.68	Pr	Nd, Eu	Gd, Dy, Tb, Ho	Er
Ce	446.02	1.58	V, Nd	Pr, Sm, Dy	Zr, Ho, Tb	Ca, Er
Pr	414.31	1.06	Y, Nd, Dy	Er, Ce	Sm, Th, Ho, Tb	La, Fe
Pr	422.30	0.56	Sr	Nd, Ce, Dy	Gd, Sm, Tb	Ca, Er, Ho
Nd	430.36	0.90	Pr	Er	Gd, Ce, Dy, Tb	Ti, Sr
Nd	415.60	1.48	Sm, Th	Pr, Ce	Gd, Dy, Ho, Tb	
Sm	443.43	1.18		Eu, Tb	Pr, Nd, Ce, Cd	Ca, La, Ti, Ho
Sm	442.43	0.73	Pr	Ce, Nd	Gd, Tb, Ho, Er	Ti, Th
Eu	381.97	0.06		Nd	Sm	Fe, Gd, Ce, Pr
Eu	412.97	0.10			Nd, Sm, Dy	Gd, Pr, Ce, Ba
Gd	342.25	0.39	Ce, Dy, Ho	Tb, Er	Sm, Pr, Nd, Th	Eu
Gd	335.05	0.68	Ti, Ho, Er	Sc, Tb, Dy	Nd, Sm, Pr, Th	Ce, Ca, Eu
Tb	350.92	0.52	Ho		Nd, Sm, Th, Dy	Gd, Ce, Er, Eu
Tb	367.64	1.03	Dy, Er		Pr, Nd, Ce, Sm	Ho, Fe, Gd, Mo
Dy	353.17	0.20			Tb, Ho, Nd	Ce, Th, Pr, Sm
Dy	340.78	0.61	Gd	Ho	Tb, Zr, Er, Th	Sm, Nd, Pr, Y
Ho	345.60	0.13		Zr	Tb, Dy, Sm, Pr	Nd, Gd, Th, Er
Ho	339.90	0.29	Tb		Dy, Nd, Er, Gd	Ce, Sm, Pr, Th
Er	337.28	0.20	Ti, Tb, Sc		Dy, Ho	Th, Gd, Br, Sm
Er	349.91	0.35	Ho	Dy, Pr	Nd, Th, Zr	Tb, Y, Ti, Sm
Tm	313.13	0.24		Er, Tb, Ho	Th, Pr, Dy	Nd, Ti, Gd, Eu
Tm	346.22	0.26	Ho		Dy, Gd, Tb, Pr	Sm, Nd, Er, Ti
Yb	328.94	0.021				Er, Nd, Dy, Pr
Yb	369.42	0.044		Sm	Er, Gd, Dy	Th, Nd, Pr, Tb
Lu	261.54	0.054		Fe		Yb, Th, Ca, Dy
Lu	291.14	0.28		Th, Er, Yb	Tb, Dy, Ho	Eu, Sm, Gd
Y	371.03	0.042			Dy	Er, Ho, Yb, Tb
Y	360.07	0.047			Tb, Er, Dy	

Method of Determination of R.E.E.

Determination of R.E.E. and some accompanying elements in ores and concentrates of R.E.E. represents a combination of simultaneous (Ca, Sr, Ba, Fe, Ti and Y – fixed channels, Sm – movable detector) and sequential (other R.E.E. and Th) analysis of sample solutions prepared by acid dissolution and alkalic fusion. The above mentioned common elements are determined for corrections of spectral interferences. Of all elements, Sm exhibits minimum mutual spectral interferences with common elements and Y.

Optimum working conditions: Power input 1 200 W, argon flows (l min^{-1}): F_p = 18.3, F_a = 0.43, F_c = 1.06, carrier gas humidified, observation height 16 mm above the coil. Signal integration 10 s with 60 s preflush, 2 measurements for each sample.

Analytical lines: Optimum analytical lines with detection limits are listed in Table VIII and lines used for described determination are denoted with letter A. Following fixed channels are available for common elements: Y II 371.030, Ca II 315.887, Sr I 460.733, Ba II 455.403, Fe I 302.063, Ti II 368.519. Ca and Tm lines are measured in the 2nd order.

Calibration, interferences, precision and limits of determination: Concentration interval up to 10 or 20-fold of the background equivalent concentration of particular R.E.E. was covered with single-element calibration solutions on six equidistantly distri-

TABLE VIII
Detection limits in pure solutions ($c_L \approx 3\ s_B$) for optimum analytical lines of REE[a]

Analytical line, nm			c_L, ng ml^{-1}	Analytical line, nm			c_L, ng ml^{-1}
La II	398.852	A	5	Tb II	350.917	A	8
La II	408.672		5	Tb II	367.635		15
Ce II	413.765	A	25	Dy II	353.170	A	3
Ce II	446.021		24	Dy II	340.779		9
Pr II	422.298	A	10	Ho II	345.600	A	2
Pr II	413.314		16	Er II	349.910	A	5
Nd II	430.358		15	Er II	390.634		3
Nd II	415.608	A	23	Tm II	313.126	A	3
Sm II	443.432	A	17	Tm II	346.220		4
Sm II	442.43		10	Yb II	328.937	A	0.3
Eu II	381.967	A	1	Yb II	369.419		0.3
Eu II	412.970		2	Lu II	261.139	A	1
Gd II	335.047	A	10				
Gd II	342.247		6				
Y II	371.030	A	0.3				

[a] Lines denoted with A were used for the analysis.

buted concentration levels including zero. Measurement of each calibration solution was repeated six times. Statistical evaluation of the calibration plot without background subtraction yielded following values of the RSD (%) of concentration: 10, 2.0 and 0.8 on concentration levels (*BEC*)/10, *BEC* and 10 × (*BEC*), respectively. These values of the RSD do not differ significantly for various R.E.E.. The spectrometer was calibrated using two concentration levels, low and high point, during routine analysis. Concentrations of single-element calibration solutions for sequential measurement were (mg l^{-1}): high point – 25 La, 50 Ce, 5 Pr, 10 Nd, 2 Eu, 2 Gd, 2 Tb, 2 Dy, 2 Ho, 2 Th, 1 Er, 1 Tm, 1 Yb, 1 Lu; low point – 5 La, 10 Ce, 1 Pr, 2 Nd and blank solutions for other R.E.E. and Th. Multi-element calibration solutions for sequential measurement (mg l^{-1}): high point – one solution containing: 2 Sm, 2 Y, 100 Ca, 50 Sr, 10 Ba, 20 Ti and 20 Fe; low point – a blank solution. Solutions were prepared in 1.4 mol l^{-1} HNO_3.

Correction factors for employed lines have been published in ref.[11]. Interval estimates of both employed and alternative lines follow from Table VII. These factors were arranged into the matrix 21 × 21 for computations of net concentrations using programme VZAZEM[10,13,27] on P 855 M Philips computer. All correction factors include both the background shift and line overlap components, no background correction facility being available.

Although the RSD for precision obtained from the calibration plot is below 1%, the precision of evaluation of analytical signals is decreased by spectral corrections. The precision of determination of main constituents in ores and concentrates, e.g. Ce, La, Nd, Pr, is not very different from precision for pure single-element solutions, but in cases of Gd and other heavier R.E.E. where random errors of spectral corrections are considerably high in comparison to concentrations of these elements, the overall precision is worsened up to six times (Gd). This result is in agreement with a calculation according to the Eq. (5).

Limits of detection in real sample solutions are higher than in pure solutions, in some cases even by one order of magnitude[11]. Predicted limits of quantitative determination using Eq. (6) were confirmed on bastnesite and apatite samples[11]. It follows from obtained results of analyses of ores and concentrates that the quantitative determination can be performed for concentrations above 0.3 mg l^{-1} Ce, Pr and Sm, 0.1 mg l^{-1} Tb, Gd, La, Nd and Er, 0.03 mg l^{-1} Dy, Ho and Tm, and 0.01 mg l^{-1} Eu, Yb, Lu and Y. Accompanying elements are determined above 1 mg l^{-1} Ca, 0.1 mg l^{-1} Sr, 0.01 mg l^{-1} Ba, 0.06 mg l^{-1} Fe, 0.2 mg l^{-1} Ti and 0.2 mg l^{-1} Th.

As to the matrix interferences, only nonspecific influence of variable concentrations of acids and salts can be observed. Hence, constant concentration of the acid 1.4 mol l^{-1} HNO_3 is maintained in unknown samples as well as in calibration samples. It is also advisable to dilute a basic sample solution having the concentrations 0.5 - 1.0 wt.% for the analysis. A 50 times or 100 times dilution of this basic sample solution is used usually.

Repeatability and accuracy of results: The repeatability of determination was tested on samples of Kola-apatite, hydroxide concentrate, bastnesite and oxidic concentrate, cf. refs[11,14].

Comparative analyses were carried out using various analytical techniques: AAS, XRF, DCP-OES, spectrophotometry[11,14]. Accuracy of the results was verified using Student's test and the orthogonal regression[42]. Using Student's test, it was proved that there were no statistically significant differences between our results and results obtained with direct current plasma spectrometer (DCP-OES) at the Institute of Mineral Resources in Kutná Hora, The Czech Republic, cf. refs[11,14].

Orthogonal regression analysis was applied on 14 following samples: Kola-apatite 066/85, hydroxide concentrates 086/85 and 011/83, oxidic concentrate 089/85, bastnesite-parisite ores from Vietnam NNX-9, BNX-IV/8, BNX-II/13, BNX-I/8, BNX-III/5, and DP, bastnesite 097/85, bastnesite ore from Syria BS, hydroxide concentrate of bastnesite 012/83 and monazite MON. Results taken for the regression were average values of 3 to 30 determinations for each sample obtained with ICP-OES and compa-

TABLE IX
Examples of data used for orthogonal regression[a]

Sample	Content of oxide (%) in solid sample							
	La_2O_3		CeO_2		Pr_6O_{11}		Nd_2O_3	
	OES ICP	Compar. method[b]	OES ICP	Compar. method[b]	OES ICP	Compar. method[b]	OES ICP	Compar. method[b]
066/85	0.28	0.27	0.43	0.44	0.06	0.04	0.13	0.14
086/85	25.41	25.43	41.27	41.75	5.17	5.03	17.29	16.81
089/85	27.25	27.21	46.47	46.13	4.16	4.17	12.53	12.95
097/85	22.78	22.85	35.19	35.20	2.85	2.93	7.82	7.97
011/83	22.69	22.38	49.05	49.12	4.09	3.91	13.73	14.06
012/83	28.13	28.16	31.42	31.39	4.06	4.04	12.21	12.85
BS	8.54	8.48	11.98	12.44	1.16	1.28	3.50	3.63
MON	2.51	2.35	5.80	5.84	0.63	0.63	2.23	2.14
NNX-9	5.59	5.68	9.18	9.13	0.86	0.84	2.43	2.45
BNX-IV	0.96	0.94	2.25	2.27	0.25	0.26	0.85	0.83
BNX-II	2.38	2.36	3.82	3.79	0.38	0.36	0.90	0.91
BNX-I	1.02	1.05	1.76	1.79	0.20	0.21	0.59	0.56
BNX-III	1.40	1.36	2.50	2.48	0.27	0.25	0.68	0.71
DP	19.08	18.99	21.95	22.25	1.92	1.97	4.96	4.90

[a] Presented values are arithmetic averages calculated for sets of results containing 3 – 30 determinations.
[b] Compared method: AAS, XRF, DCP-OES, spectrophotometry.

rison techniques. Some data for regression analysis are summarized in Table IX. Prior to regression analysis, the normal distribution of data was tested. Then regression lines were calculated, slopes and intercepts tested for the significance of the difference against one and zero, respectively and parameters of contour ellipses were evaluated. A good agreement between ICP and compared results was found for the main constituents of the samples (La, Ce, Pr, Nd, Sm, Eu and Gd). For some heavy R.E.E. proportional systematic errors were observed due to over- or undercorrected results. However, in most of these cases even considerable underestimation of ICP results (15 rel.%) was insignificant due to large spread of the points along the regression line, cf. ref.[43].

Above described method has been successfully used for the determination of R.E.E. in more than 1 500 samples of concentrates, ores, samples of technological separation of individual R.E.E. which represents about 16 000 determinations.

REFERENCES

1. Walsh J. N., Buckley F., Barker J.: Chem. Geol. *33*, 141 (1981).
2. Crock G., Lichte F. E.: Anal. Chem. *54*, 1329 (1982).
3. Barnes R. M., Mahanti H. S.: Appl. Spectrosc. *37*, 261 (1983).
4. Roelandts I.: Chem. Geol. *67*, 171 (1988).
5. Roelandts I.: At. Spectrosc. 9, 49 (1988).
6. Šulcek Z., Rubeška I., Sixta V., Paukert T.: At. Spectrosc. *10*, 4 (1989).
7. Weiss D., Paukert T., Rubeška I.: J. Anal. At. Spectrosc. *5*, 371 (1990).
8. Fischer P. T., Ellgren A. J.: Spectrochim. Acta, B *38*, 309 (1983).
9. Kanický V., Toman J., Maleček M.: *7th Czechoslovak Spectroscopic Conference and VIIIth CANAS, České Budějovice 1984.* Abstract of Papers, Poster No. 49.
10. Kanický V., Toman J., Maleček M., Povolný A.: Chem. Listy *81*, 1304 (1987).
11. Kanický V., Toman J., Maleček M., Povolný A.: Chem. Listy *82*, 630 (1988).
12. Kanický V.: Chem. Listy *83*, 1095 (1989).
13. Kanický V., Toman J.: ICP Information Newsletter *15*, 444 (1990).
14. Šulcek Z., Dempír J., Kanický V., Macháček V., Maleček M., Musil J., Paukert T., Perný M., Rubeška I., Sixta V., Šimůnek P., Toman J., Weiss D.: Report A 09-347-831. Geological Survey, Prague 1987.
15. Boumans P. W. J. M., Tielrooy J. A., Maessen F. J. M. J.: Spectrochim. Acta, B *43*, 173 (1988).
16. Havel J., Moreno C., Valiente M., Hrdlička A.: *6th Czechoslovak Conference on Atomic Spectroscopy, Brno 1991.* Abstract of Papers, Poster No. 18.
17. Boumans P. W. J. M.: *Line Coincidence Tables for Inductively Coupled Plasma Atomic Emission Spectrometry.* Pergamon, Oxford 1980.
18. Parsons L. M., Forster A. R., Anderson D. L.: *An Atlas of Spectral Interferences in ICP Spectroscopy.* Plenum, New York 1980.
19. Winge R. K., Fassel V. A., Peterson V. J., Floyd M. A.: *Inductively Coupled Plasma Atomic Emission Spectroscopy – An Atlas of Spectral Information.* Elsevier, Amsterodam 1985.
20. Wysocka-Lisek J.: *Spectrum Lines of Rare Earths Arranged by Wavelengths.* Lubelske Towarz. Naukowe, Lodz 1970.
21. Gunter W. H., Visser K., Zeeman P. B.: Spectrochim. Acta, B *38*, 949 (1983).
22. Boumans P. V. J. M., Lux-Steiner M. Ch.: Spectrochim. Acta, B *37*, 97 (1982).
23. I.U.P.A.C.: Pure Appl. Chem. *51*, 1195 (1979).

24. Zaidel A. N., Prokofiev V. K., Raiski S. M., Slavnyi V. A., Sreider J.: *Tablicy spektral'nykh linii.* Nauka, Moskva 1969.
25. Matooka J. M., Mosier E. L., Sutley S. J., Viets J. B.: Appl. Spectrosc. *33*, 456 (1979).
26. Koirtyohann S. R., Jones S. J., Jester P. C., Yates D. A.: Spectrochim. Acta, B *36*, 49 (1981).
27. Povolný A., Maleček M.: *Programme VZAZEM.* Geological Survey, Brno 1982.
28. Kanický V.: Chem. Listy *83*, 84 (1989).
29. Boumans P. W. J. M., Mc Kenna J. J., Bosveld M.: Spectrochim. Acta, B *36*, 1031 (1981).
30. Prudnikov E. D., Shapkina L. S.: Chem. Anal. (Warsaw) *31*, 335 (1986).
31. Kawaguchi H., Ito T., Mizuike A.: Spectrochim. Acta, B *36*, 615 (1981).
32. Blades M. W., Horlick G.: Spectrochim. Acta, B *36*, 861 (1981).
33. Furuta M., Horlick G.: Spectrochim. Acta, B *37*, 53 (1982).
34. Edmonds T. E., Horlick G.: Appl. Spectrosc. *31*, 36 (1977).
35. Faires L. M., Palmer B. A., Engelman B., Niemczyk T.: Spectrochim. Acta, B *39*, 819 (1984).
36. Furuta N.: Spectrochim. Acta, B *41*, 1115 (1986).
37. Houk R. S., Olivarez J. A.: Spectrochim. Acta, B *39*, 575 (1984).
38. Anderson T. A., Burns D. W., Parsons M. L.: Spectrochim. Acta, B *39*, 559 (1984).
39. Rybarczyk J. P., Jester C. P., Yates D. A., Koirtyohann S.: Anal. Chem. *54*, 2162 (1982).
40. Furuta N., Nojiri Y., Fuwa K.: Spectrochim. Acta, B *40*, 617 (1985).
41. Gunter W., Visser K., Zeeman P. B.: Spectrochim. Acta, B *37*, 869 (1982).
42. Holdt G., Strasheim A.: Appl. Spectrosc. *14*, 64 (1960).
43. Kanický V.: *Ph.D. Thesis.* Masaryk University, Brno 1990.

Translation revised by H. P. Mašková.